Clim. Past Discuss., 10, 3255–3302, 2014
www.clim-past-discuss.net/10/3255/2014/
doi:10.5194/cpd-10-3255-2014

Climate of the Past
Discussions
Open Access

Using simulations of the last millennium to understand climate variability seen in paleo-observations: similar variation of Iceland-Scotland overflow strength and Atlantic Multidecadal Oscillation

K. Lohmann[1], J. Mignot[2,3], H. R. Langehaug[4,5], J. H. Jungclaus[1], D. Matei[1], O. H. Otterå[5,6], Y. Gao[4,5], T. L. Mjell[5,7], U. Ninnemann[5,7], and H. F. Kleiven[5,7]

[1]Max Planck Institute for Meteorology, Hamburg, Germany
[2]LOCEAN, Institute Pierre-Simon Laplace, University Pierre and Marie Curie, Paris, France
[3]Climate and Environmental Physics, and Oeschger Centre of Climate Change Research, University of Bern, Bern, Switzerland
[4]Nansen Environmental and Remote Sensing Center, Bergen, Norway
[5]Bjerknes Centre for Climate Research, Bergen, Norway
[6]Uni Research, Bergen, Norway
[7]Department of Earth Science, University of Bergen, Bergen, Norway

Received: 12 April 2014 – Accepted: 1 May 2014 – Published: 11 August 2014

Correspondence to: K. Lohmann (katja.lohmann@mpimet.mpg.de)

Published by Copernicus Publications on behalf of the European Geosciences Union.

Abstract

A recent paleo-reconstruction of the strength of the Iceland-Scotland overflow during the last 600 years suggests that its low-frequency variability exhibits strong similarity with paleo-reconstructions of the Atlantic Multidecadal Oscillation (AMO). The underlying mechanism of the apparent covarying remains, however, unclear based on paleo-reconstructions alone. In this study we use simulations of the last millennium driven by external forcing reconstructions with three coupled climate models in order to investigate possible mechanisms underlying the apparent covarying. Two of the model simulations show a clear in-phase variation of Iceland-Scotland overflow strength and AMO index. Our analysis indicates that the basinwide AMO index in the externally forced simulations is dominated by the low-latitude SST variability and is not predominantly driven by variations in the strength of the Atlantic meridional overturning circulation (MOC). In the simulations, also a strong (weak) Iceland-Scotland overflow does generally not lead a strong (weak) MOC, suggesting that a large-scale link through the strength of the MOC is not sufficient to explain the (simulated) in-phase variation of Iceland-Scotland overflow strength and AMO index. Rather, a more local link through the influence of the Nordic Seas SST, which is positively correlated with the AMO index, on the Iceland-Scotland overflow strength is responsible for the (simulated) in-phase variation. The Nordic Seas surface state affects, via convective activity, the density structure and the sea surface height (SSH), and consequently the pressure north of the Iceland-Scotland-Ridge. In the model simulation showing a less clear in-phase variation of Iceland-Scotland overflow strength and AMO index, also the wind stress influences the Nordic Seas SSH anomalies associated with the anomalous overflow strength. The details of the mechanisms differ between the three models, underlining the importance of multi-model analysis. Our study demonstrates that paleo-climate simulations provide a useful tool to understand mechanisms and large-scale connections associated with the relatively sparse paleo-observations.

CPD
10, 3255–3302, 2014

1 Introduction

Marine sediment cores provide paleo-climatic information by allowing the reconstruction of marine quantities back in time. Apart from temperature and salinity, which are deduced from the chemical properties of plankton shells, the strength of the near-bottom flow can also be reconstructed based on the mean sediment grain-size (with larger grain-size corresponding to stronger near-bottom flow), if the sediment cores are taken along sediment drifts, where there is lateral transport and input of sediments. Due to this lateral sediment transport by deep-ocean currents, the pattern of oceanic sediment drifts mirrors the path of the deep-ocean currents (Wold, 1994). Recently, a reconstruction of the Iceland-Scotland overflow strength for the last 600 years has become available (Mjell et al., 2014a) based on a sediment core located downstream of the Iceland-Scotland-Ridge (ISR), within the Gardar sediment drift at the eastern flank of the Reykjanes Ridge. The reconstructed overflow time series exhibits pronounced variability on multidecadal to centennial time scales, which agrees well with the variability suggested from a previous study by Boessenkool et al. (2007) based on the mean sediment grain size from a sediment core spanning the last 250 years, which is located downstream of the core discussed in Mjell et al. (2014a).

Mjell et al. (2014a) further reveal a strong similarity between the low-frequency variability of the Iceland-Scotland overflow strength and reconstructions (e.g. Gray et al., 2004) of the Atlantic Multidecadal Oscillation (AMO), with periods of strong flow associated with Atlantic-wide warmth (our Fig. 1, adapted from their Fig. 2c). The AMO is the leading mode of sea surface temperature (SST) variability in the North Atlantic on multidecadal time scales (e.g. Schlesinger and Ramankutty, 1994, based on temperature records; Delworth and Mann, 2000, based on temperature records and coupled climate models). Paleo-reconstructions are, however, still very rare and do not allow a detailed investigation of mechanisms underlying the (co)variability suggested from them.

CPD
10, 3255–3302, 2014

A broader insight into the paleo-climate can be provided by coupled climate model simulations driven by external forcing reconstructions, such as variations in the solar irradiance or major volcanic eruptions. AMO and North Atlantic SST variability in general as well as some aspects of the oceanic circulation, such as the North Atlantic gyre and especially the Atlantic meridional overturning circulation (MOC), in externally forced simulations have recently been discussed in the literature. Previous studies, based on various coupled climate models and external forcing reconstructions from different sources, address the impact of both solar variability (e.g. Goosse and Renssen, 2006; Swingedouw et al., 2011; Park and Latif, 2012) and volcanic aerosols (e.g. Stenchikov et al., 2009; Otterå et al., 2010; Mignot et al., 2011; Ortega et al., 2012; Zhong et al., 2011; Zanchettin et al., 2012, 2013a). They arrive, however, at partly contradictory conclusions. Attempts to explain the differences in the oceanic response to external forcing point towards a dependence on the simulated background state (Zanchettin et al., 2012) as well as on the frequency of major volcanic eruptions in the time period considered for the analysis (Mignot et al., 2011). Reconstructions of external forcing components are also subject to some debate, such as the amplitude of solar radiation variability. In contrast to North Atlantic SST and MOC, the overflow from the Nordic Seas through the Denmark Strait and across the ISR has not been (much) studied in externally forced simulations.

Here we use simulations of the last millennium driven by external forcing reconstructions with three coupled climate models to investigate mechanisms underlying the apparent covarying of Iceland-Scotland overflow strength and AMO index suggested from paleo-reconstructions (Mjell et al., 2014a). Two possible mechanisms linking the two time series are discussed: (i) a large-scale link through the strength of the MOC in the sense that a strong [weak] Iceland-Scotland overflow leads to a strong [weak] MOC which leads to a warm [cold] phase of the AMO. There is evidence from previous studies based on ocean reanalysis and control simulations with coupled climate models for an influence of the Denmark Strait overflow variability on the variability of the MOC (e.g. Jungclaus et al., 2005; Köhl and Stammer, 2008)

CPD
10, 3255–3302, 2014

as well as for the association of multidecadal SST anomalies in the North Atlantic, as reflected in the AMO index, with multidecadal MOC variations (e.g. Delworth and Mann, 2000; Latif et al., 2004; Knight et al., 2005). Mechanism (ii) consists of a more local link through the influence of the Nordic Seas SST, which is positively correlated with the basinwide AMO index as discussed below, on the pressure north of the ISR. Previous observational (e.g. Hansen et al., 2001) and modelling (e.g. Jungclaus et al., 2008) studies suggest that the overflow transport through the Faroe-Shetland-Channel (FSC), which carries the majority of the overflow between Iceland and Scotland, is controlled by internal hydraulics and affected by the baroclinic pressure gradient across the ISR in the core depth of the overflow. Further observational (e.g. Hansen and Østerhus, 2007) and modelling (e.g. Olsen et al., 2008; Sandø et al., 2012) studies add the importance of the barotropic pressure gradient. Note that mechanism (ii) also involves the MOC through the transport of heat and salt from the subtropics into the Nordic Seas.

Our study is organized as follows: The models and the experimental set-up as well as the simulated Iceland-Scotland overflow strength and AMO index are described in Sect. 2. In Sect. 3, the two possible mechanisms underlying the in-phase variation of Iceland-Scotland overflow strength and AMO index introduced above are investigated. The results are discussed in Sect. 4 and the main conclusions are given in Sect. 5.

2 Model description and simulated variability of Iceland-Scotland overflow strength and AMO index

2.1 Model description and experimental set-up

Our study is based on simulations of the last millennium driven by external forcing reconstructions conducted with three global coupled climate models, namely the Max Planck Institute for Meteorology Earth System Model (MPI-ESM), the coupled climate model developed at the Institute Pierre-Simon Laplace (IPSLCM4 v2, hereafter IPSLCM4) and the Bergen Climate Model (BCM). These model simulations were made

CPD
10, 3255–3302, 2014

available within the EU-project THOR (ThermoHaline Overturning – at Risk?). We limit our study to model simulations from the project partners, as non-standard model output, such as the overflow transport across the ISR, is needed.

In MPI-ESM, the atmosphere general circulation model (GCM) ECHAM6 (Stevens et al., 2013) is coupled to the ocean/sea ice GCM MPIOM (Marsland et al., 2003; Jungclaus et al., 2013; Notz et al., 2013), using the OASIS3 coupler (Valcke et al., 2003). The carbon cycle in MPI-ESM comprises the ocean biogeochemistry module HAMOCC5 (Ilyina et al., 2013) and the land surface scheme JSBACH (Reick et al., 2013). The atmosphere GCM is run at a horizontal resolution of T63 (spectral grid with truncation at wave number 63; corresponding to about 1.875° on a Gaussian grid) and 47 vertical levels, resolving the stratosphere up to 0.01 hPa. The ocean GCM applies a conformal mapping grid in the horizontal with the North Pole shifted to southern Greenland (to circumvent grid singularities in the computational ocean domain), featuring a nominal resolution of 1.5°. The convergence of the mesh-size towards the poles translates into a grid spacing of 15 to 100 km in the North Atlantic. Vertically, 40 unevenly spaced z levels are used with the first 20 levels covering the upper 700 m of the water column.

In IPSLCM4 (Marti et al., 2010), the atmosphere GCM LMDz4 (Hourdin et al., 2006) and the ORCHIDEE module for continental surfaces (Krinner et al., 2005) are coupled to the ocean GCM OPA8.2 (Madec et al., 1998) and the sea ice model LIM2 (Fichefet and Maqueda, 1997), using the OASIS2.4 coupler (Valcke et al., 2000). The atmosphere GCM is run at a horizontal resolution of 3.75° (in longitude) × 2.5° (in latitude) and 19 vertical levels, resolving the stratosphere up to 3 hPa. The ocean GCM uses the ORCA2 grid in the horizontal, i.e. a conformal mapping, tripolar grid with two poles placed in the northern hemisphere over land (American and Asian continents respectively) to avoid grid singularities in the computational ocean domain. The averaged horizontal resolution is 2° with the meridional grid spacing refined to 0.5° around the equator (to better resolve the dynamics near the equator). The convergence of the mesh-size towards the poles translates into a grid spacing of about 100 to 200 km

CPD
10, 3255–3302, 2014

in the North Atlantic. Vertically, 31 unevenly spaced z-levels are used with the first 20 levels covering the upper 600 m of the water column.

In BCM (Furevik et al., 2003; Otterå et al., 2009), the atmosphere GCM ARPEGE (Deque et al., 1994) is coupled to the ocean GCM MICOM (Bleck and Smith, 1990; Bleck et al., 1992) and the sea ice model GELATO (Salas-Melia, 2002), using the OASIS (version 2) coupler (Terray and Thual, 1995). In the MICOM model used in BCM, several important aspects deviate from the original model (e.g. Otterå et al., 2009), most important the conservation of heat and salt gained by introducing incremental remapping (Dukowicz and Baumgardner, 2000) for the advection of tracers. The atmosphere GCM is run at a horizontal resolution of T63 (spectral grid with truncation at wave number 63; corresponding to about 1.875° on a Gaussian grid) and 31 vertical levels, resolving the stratosphere up to 10 hPa. The ocean GCM applies a conformal mapping grid in the horizontal with the North Pole located over Siberia to avoid grid singularities in the computational ocean domain, featuring a nominal resolution of 2.4° with the meridional grid spacing near the equator being gradually decreased up to 0.8° at the equator (to better resolve the dynamics near the equator). The grid spacing in the North Atlantic amounts to about 150 to 200 km. Vertically, 34 isopycnal layers with potential densities ranging from $\sigma_2 = 30.119$ to $37.800\,\mathrm{kg\,m^{-3}}$ and on top of them a non-isopycnic surface mixed layer are used.

With respect to the simulated decadal to centennial scale climate variability in the North Atlantic, recent multi-model control simulation studies (including the three models used here) discuss differences for the different coupled climate models in both the representation of the low-frequency North Atlantic climate variability as well as in the mechanisms and feedbacks involved (e.g. Menary et al., 2012; Langehaug et al., 2012b; Gastineau and Frankignoul, 2012; Ba et al., 2014).

Regarding the external forcing reconstructions used to force the model simulations, volcanic aerosols are based on reconstructions by Crowley et al. (2008) in the MPI-ESM simulation, Ammann et al. (2003) and Gao et al. (2008) in the IPSLCM4 simulation and Crowley et al. (2003) in the BCM simulation. The volcanic aerosols

CPD
10, 3255–3302, 2014

are distributed over a couple of stratospheric levels and the effect on the radiative forcing is calculated online in all models. For the solar forcing, a weak scaling based on total solar irradiance (TSI) reconstructions by Vieira and Solanki (2010) and Vieira et al. (2011) is used in the MPI-ESM and IPSLCM4 simulation, with an increase in TSI of 0.1 % from the 17th century Maunder Minimum to present time. A weak scaling of solar forcing is recommended in the protocol of the third phase of the Paleoclimate Modelling Intercomparison Project (PMIP3; Schmidt et al., 2011). In the BCM simulation, a TSI reconstruction based on Crowley et al. (2003) is used, which exhibits a stronger amplitude compared to the one used in the other two models. Changes in orbital parameters are taken into account in the MPI-ESM and IPSLCM4 simulation, but are not included in the BCM simulation.

With respect to anthropogenic forcing, the most important well-mixed greenhouse gases are taken into account in the MPI-ESM and IPSLCM4 simulation. In the MPI-ESM simulation, also land cover changes (Pongratz et al., 2008) and anthropogenic aerosols are considered. In the IPSLCM4 simulation, the vegetation is set to modern climatology from Myneni et al. (1997). Anthropogenic aerosol forcing is not included in the IPSLCM4 simulation, leading to a stronger warming trend in the recent decades compared to the MPI-ESM simulation and reconstructions. In the BCM simulation, no anthropogenic forcing components are included. We note, however, that the discussion of possible differences in the model simulations due to differences in the external forcing components is beyond the scope of this study. The discussion of possible mechanisms underlying an in-phase variation of Iceland-Scotland overflow strength and AMO index is limited to the pre-industrial period in the MPI-ESM and IPSLCM4 simulation, mainly excluding the effect of the anthropogenic forcing components.

For MPI-ESM, a 400-year adaptation run, starting from the pre-industrial control simulation as described in Jungclaus et al. (2013), is performed under orbital forcing conditions representing the year AD 850. Afterwards, the externally forced simulation is performed for the period AD 850 to 1850, followed by a "historical" simulation (years AD 1850 to 2005) according to the protocol of the fifth phase of the Coupled Model

CPD
10, 3255–3302, 2014

Intercomparison Project (CMIP5). For a more detailed description of the external forcing used in the MPI-ESM simulation, we refer the reader to Jungclaus et al. (2010) and Schmidt et al. (2011). For IPSLCM4, after a spin-up phase of 310 years, the externally forced simulation is performed for the period AD 850 to 2000. For a more detailed description of the simulation we refer the reader to Mignot et al. (2011) and references therein. Note that this simulation was part of PMIP2 and differs from the one included in the more recent PMIP3. For BCM, after a spin-up phase of 500 years (Otterå et al., 2009), the externally forced simulation is performed for the period AD 1400 to 2000. For a more detailed description of the simulation we refer the reader to Otterå et al. (2010) and references therein.

In this study we focus on the low-frequency variability of the Iceland-Scotland overflow strength and the AMO index. Therefore, all model data are annual values (or seasonal values for variables such as the mixed layer depth) with a 21-year running mean lowpass-filter applied.

2.2 Iceland-Scotland overflow strength and AMO index in the simulations

Here we define the Iceland-Scotland overflow strength and the AMO index as well as investigate their variability in the three last-millennium simulations presented above. The reconstruction from Mjell et al. (2014a) represents the strength of the near-bottom current at the eastern flank of the Reykjanes Ridge along the flow path of the Iceland-Scotland overflow water. In the models, we have access to the full velocity field and can thus also estimate the strength of the Iceland-Scotland overflow directly. The latter is defined as the total transport out of the Nordic Seas across the ISR with a density threshold of $\sigma > 27.8\,\mathrm{kg\,m^{-3}}$ in MPI-ESM and IPSLCM4 and as the net transport across the ISR with a density threshold of $\sigma_2 > 36.946\,\mathrm{kg\,m^{-3}}$ in BCM. In the latter, the density threshold is specified as σ_2 value, because in the ocean component σ_2 isopycnal coordinates are used. We note that the difference in defining the overflow across the ISR as transport of the Nordic Seas or as net transport is negligible, as a transport into the Nordic Seas with the given density threshold generally does not

CPD
10, 3255–3302, 2014

exist. Mean overflow transports amount to 3.0 Sv (1 Sverdrup = $10^6\,m^3\,s^{-1}$) in MPI-ESM, 2.7 Sv in IPSLCM4 and 3.6 Sv in BCM, which is in reasonable agreement with observational estimates of about 3.5 Sv (e.g. Hansen et al., 2008). In MPI-ESM and BCM, the overflow transport across the ISR is, in contrast to observations, restricted to the FSC, while in IPSLCM4 an overflow transport of 0.5 Sv is found between Iceland and the Faroe Plateau. One major bias in the three model simulations used here concerns the flow path of the Iceland-Scotland overflow water south of the ISR, which is not realistically simulated in the (relatively coarse-resolution) model configurations (e.g. Langehaug et al., 2012a). In contrast to observations, most of the Iceland-Scotland overflow water spreads southward in the eastern North Atlantic basin, rather than flowing around the Reykjanes Ridge (through fracture zones in the Mid Atlantic Ridge) and joining the Denmark Strait overflow water and the deep western boundary current.

In Fig. 2 we compare the simulated Iceland-Scotland overflow strength following our definition (red lines) with the simulated speed of the near-bottom current (black lines) along the eastern flank of the Reykjanes Ridge at about the same location as the sediment core (23°58′ W, 60°19′ N; Fig. 1). The low-frequency variability of the two time series agrees reasonably in all three models, with significant correlation coefficients of 0.64 in MPI-ESM, 0.52 in IPSLCM4 and 0.74 in BCM (0.59 in BCM if the first 150 integration years exhibiting a rather strong model drift are excluded). This result suggests that the (simulated) near-bottom current along the eastern flank of the Reykjanes Ridge can in general be interpreted as representing the strength of the Iceland-Scotland overflow at the exit of the Nordic Seas on time scales greater than 20 years. Regarding the BCM simulation, Mjell et al. (2014b) suggest that the simulated speed of the near-bottom current along the eastern flank of the Reykjanes Ridge is influenced by both strength and density of the Iceland-Scotland overflow. We note that the simulated speed of the near-bottom current in Fig. 2 is based on a single grid cell, but conclusions do not change if the speed is averaged along the eastern

CPD
10, 3255–3302, 2014

flank of the Reykjanes Ridge. For the discussion below, we use the overflow strength at the ISR.

The AMO index we define as the area-average of basinwide North Atlantic SST encompassing the region 75 to 7.5° W and 0 to 60° N, following Otterå et al. (2010). The latter does not include the Nordic Seas, which is important for the variability of the Iceland-Scotland overflow strength as discussed below. However, AMO index and Nordic Seas SST in the model simulations are positively correlated as discussed below and the conclusions of our study do not change if the AMO index is based on a larger region encompassing the Nordic Seas. We note also that in this definition of the AMO index, the influence of (natural and anthropogenic) external forcing is not removed, as opposed to definitions by e.g. Knight et al. (2005) or Trenberth and Shea (2006).

In Fig. 3 we compare the simulated Iceland-Scotland overflow strength and AMO index with the respective reconstruction from Mjell et al. (2014a) and Gray et al. (2004). We note that there are other AMO reconstructions available (e.g. Delworth and Mann, 2000; Mann et al., 2009). A detailed comparison of the different reconstructions, which to the best of our knowledge does not exist in the literature, would be of much interest, but is beyond the scope of our study. The simulated and reconstructed AMO index (left panels) coincide mainly in the cold periods following major volcanic eruptions, indicating that the AMO index is influenced by the external forcing, as stated in e.g. Otterå et al. (2010) and Zanchettin et al. (2013a). Concerning the Iceland-Scotland overflow strength (right panels), the agreement between the simulated and reconstructed time series is quite weak in MPI-ESM and BCM. In IPSLCM4, the simulated and reconstructed time series generally agree in the phasing of periods with strong and weak overflow, suggesting that in this model the external forcing has a stronger influence on the overflow strength than in the other two models.

The relation between the low-frequency variability of the Iceland-Scotland overflow strength and the AMO index in the three models is shown in Fig. 4. In MPI-ESM and IPSLCM4, a clear in-phase variation, as suggested by the paleo-reconstructions, is found, with zero lag correlation coefficients between the two time series for the

CPD
10, 3255–3302, 2014

pre-industrial period (years AD 850 to 1849) of 0.67 in MPI-ESM and 0.74 in IPSLCM4. It is also interesting to note that in these two models cold events related to major volcanic eruptions (e.g. around years AD 1258 and 1815) go along with weak overflow events. In BCM, an in-phase variation is less clear than in the other two models with the zero lag correlation coefficient (0.39) just above the significance level. In this model, the correlation coefficient increases to 0.53, if the AMO index leads the overflow strength by 13 years.

As indicated above, for the discussion of possible mechanisms underlying the (simulated) in-phase variation of Iceland-Scotland overflow strength and AMO index, the analysis is limited to the pre-industrial period (years AD 850 to 1849) in MPI-ESM and IPSLCM4 to avoid the 20th century warming signal due to the anthropogenic greenhouse gas forcing. In IPSLCM4, all data are additionally linearly detrended to reduce the influence of model drift (due to the relatively short spin-up phase), following Servonnat et al. (2010) and Mignot et al. (2011). The BCM simulation does not include anthropogenic forcing, but shows a rather strong model drift during the first two centuries (Figs. 2c and 4c; Otterå et al., 2009). Therefore, the analysis is limited to the period between years AD 1550 and 1999.

3 Investigation of possible mechanisms underlying the in-phase variation of Iceland-Scotland overflow strength and AMO index

In this section we will investigate the two mechanisms proposed in the introduction as possible explanation for the in-phase variation of Iceland-Scotland overflow strength and AMO index, detected in at least two models. These mechanisms are (i) a large-scale link through the strength of the MOC and (ii) a more local link through the influence of the Nordic Seas surface state on the Iceland-Scotland overflow strength.

CPD
10, 3255–3302, 2014

3.1 Mechanism (i): Iceland-Scotland overflow strength and AMO index linked through the strength of the MOC?

Mechanism (i) suggests an in-phase variation of Iceland-Scotland overflow strength and AMO index due to a strong [weak] overflow leading to a strengthening [weakening] of the MOC which leads to a warm [cold] phase of the AMO.

Figure 5 shows the lag correlation between the Iceland-Scotland overflow strength and the strength of the MOC as a function of the different latitudes in the North Atlantic (at the depth where the absolute maximum strength of the North Atlantic MOC is located) in the three models. All depicted correlation coefficients are statistically significant at the 95 % confidence level. No robust relation in the sense that a strong [weak] Iceland-Scotland overflow leads a strong [weak] MOC is detectable from this figure. In MPI-ESM (Fig. 5a), Iceland-Scotland overflow strength and MOC (mainly at subpolar latitudes) are negatively correlated when the MOC is lagging the overflow. IPSLCM4 (Fig. 5b) shows (weak) positive correlation coefficients when the MOC is lagging, although at rather long lags (more than 25 years) and not in the lower branch of the MOC (not shown) as one might expect if the MOC variability would be caused by the overflow variations. In BCM (Fig. 5c), no significant correlation coefficients are found with the MOC lagging. In addition, a strengthening of the MOC following major volcanic eruptions is described in several previous modelling studies (e.g. Otterå et al., 2010, analysing the same BCM simulation as used in our study; Zanchettin et al., 2012, analysing simulations of the last millennium with a coarser-resolution MPI-ESM configuration), while the Iceland-Scotland overflow strength is at a minimum during major volcanic eruptions (e.g. in years AD 1258 and 1815; Fig. 4). A robust relation between the Iceland-Scotland overflow strength and the MOC is also not found in a multi-model control simulation study (including the three models used here) investigating the sensitivity of the MOC to variations in the overflows from the Nordic Seas (Lohmann et al., 2014). The latter study rather points towards a higher correlation between the Denmark Strait overflow strength and the MOC. The influence of the

CPD
10, 3255–3302, 2014

Iceland-Scotland overflow strength on the MOC might, however, be underestimated in the model simulations, as the models do not realistically simulate the flow path of the Iceland-Scotland overflow water south of the ISR (Sect. 2.2).

The correlation between the maximum strength of the North Atlantic MOC (leading by a few years) and the North Atlantic SST in the three models is shown in the right panels in Fig. 6. The maximum strength of the North Atlantic MOC is located at about 30° N in MPI-ESM, 35° N in BCM and 45° N in IPSLCM4 at a depth of about 1000 m, respectively. We note that the conclusions from Fig. 6 do not change if a fixed latitude of 30° N is used for all models. The largest influence of the low-frequency MOC variability on the North Atlantic SST is found, in MPI-ESM and BCM, in the subpolar region, in agreement with studies based on control simulations (e.g. Latif et al., 2004). In MPI-ESM (Fig. 6b), the significant influence of the MOC on the North Atlantic SST is limited to this region, while in BCM (Fig. 6f) a significant influence is also found on the SST in the Nordic Seas. In IPSLCM4 (Fig. 6d), almost no significant influence of the MOC on the North Atlantic SST is found at all. We note that in MPI-ESM and IPSLCM4, this differs from the behaviour in the respective control simulation, where the correlation between the maximum strength of the North Atlantic MOC and the North Atlantic SST (not shown) also includes significant correlation coefficients in the Nordic Seas, the subtropics and (in IPSLCM4) the subpolar region, consistent with e.g. Zanchettin et al. (2013b, MPI-ESM) and Msadek and Frankingnoul (2009, IPSLCM4). In BCM, the influence of the MOC on the North Atlantic SST is similar in the control and the externally forced simulation. These findings indicate that in MPI-ESM, and especially in IPSLCM4, the MOC signature on the North Atlantic SST is reduced in the externally forced simulations due to the influence of the external radiative forcing on the SST. Consistently, C. Marini (personal communication, 2013), analysing the same IPSLCM4 simulation as used in our study, finds a higher correlation between the AMO and the MOC if a mode representing the response to volcanic forcing is removed from the AMO.

The (zero lag) correlation between the AMO index and the North Atlantic SST is shown in the left panels in Fig. 6. The highest correlation coefficients are, in all three models, found in the tropical and subtropical region, with maximum correlation coefficients of 0.8 in BCM (Fig. 6e), 0.85 in MPI-ESM (Fig. 6a) and larger than 0.9 in IPSLCM4 (Fig. 6c). This indicates that in the framework of the last millennium, the basinwide North Atlantic SST variability, as reflected in the AMO index, is dominated by the relatively large (sub)tropical North Atlantic region as stated in Otterå et al. (2010). The SST in the (sub)tropical regions is indeed largely influenced by the relevant external radiative forcing of the last millennium (solar and volcanic forcing), as suggested in previous modelling studies (e.g. Otterå et al., 2010; Mignot et al., 2011; Terray, 2012). For the SST in the Nordic Seas, which is important for the Iceland-Scotland overflow strength as discussed below, correlation coefficients are of comparable magnitude in MPI-ESM and IPSLCM4, reaching maximum values of 0.7 (Fig. 6a and c). In BCM (Fig. 6e), correlation coefficients between the AMO index and the Nordic Seas SST are weaker compared to the other two models.

The lowest correlation coefficients between the AMO index and the North Atlantic SST are found in the subpolar region (left panels in Fig. 6). This finding is robust within the three models and is also seen in Zanchettin et al. (2013a) using the reconstructed AMO index from Gray et al. (2004) and simulations of the last millennium with a coarser-resolution MPI-ESM configuration. The region, where the lowest correlation coefficients between the AMO index and the North Atlantic SST are found (left panels in Fig. 6) coincides, in all three models, with the region where the highest correlation coefficients between the maximum strength of the North Atlantic MOC and the North Atlantic SST are found (right panels in Fig. 6). This suggests that in the externally forced simulations the basinwide AMO index, which is dominated by the low-latitude SST variability, is not predominantly driven by MOC changes.

From the results presented in this section we conclude that mechanism (i), a link through the strength of the MOC, is not sufficient to explain the (simulated) in-phase variation of Iceland-Scotland overflow strength and AMO index.

CPD
10, 3255–3302, 2014

3.2 Mechanism (ii): AMO index and Iceland-Scotland overflow strength linked through the influence of the Nordic Seas surface state on the Iceland-Scotland overflow strength?

Mechanism (ii) implies that the in-phase variation of Iceland-Scotland overflow strength and AMO index is due to the influence of the Nordic Seas SST, which is positively correlated with the AMO index (left panels in Fig. 6), on the pressure north of the ISR. According to the literature (e.g. Hansen and Østerhus, 2007; Jungclaus et al., 2008; Olsen et al., 2008; Sandø et al., 2012), the latter affects the strength of the Iceland-Scotland overflow.

The correlation between the Iceland-Scotland overflow strength and the northeastern North Atlantic SST in the three models is shown in Figs. 7a, 8a and 9a. Maximum correlation coefficients are found at zero lag in MPI-ESM and for the overflow lagging by two and nine years in IPSLCM4 and BCM respectively. Strong Iceland-Scotland overflow is associated with an anomalously warm surface state in the Nordic Seas. Maximum correlation coefficients reach about 0.85 in MPI-ESM (Fig. 7a), 0.7 in IPSLCM4 (Fig. 8a) and 0.6 in BCM (Fig. 9a). Positive correlation coefficients are also found south of the Greenland-Scotland-Ridge (GSR) in MPI-ESM and IPSLCM4, and south of the ISR in BCM.

The correlation between the Iceland-Scotland overflow strength and the northeastern North Atlantic sea surface salinity (SSS) is shown in Figs. 7b, 8b and 9b. Strong Iceland-Scotland overflow is associated with an anomalously salty surface state in the Nordic Seas, with maximum correlation coefficients of similar order as for SST. In contrast to SST, positive correlation coefficients between the Iceland-Scotland overflow strength and the SSS do, in principal, not extend south of the GSR. Also in contrast to SST, negative correlation coefficients are found in the northwestern part in MPI-ESM (Fig. 7b) and IPSLCM4 (Fig. 8b) and in the region close to the Norwegian coast in MPI-ESM, where an anomalously fresh surface state is associated with strong Iceland-Scotland overflow. The SSS anomalies in the northwestern part of the Nordic Seas are

CPD
10, 3255–3302, 2014

related to less sea ice extent under warmer conditions (not shown), while the reason for the anomalies close to the Norwegian coast is not clear.

In the following, we first describe processes that contribute to the anomalously warm and salty Nordic Seas surface state associated with strong Iceland-Scotland overflow, and afterwards how these anomalies can, in turn, affect the overflow strength. Only the case of strong Iceland-Scotland overflow is discussed, but the described mechanism is linear and opposite conclusions can be drawn for the case of weak overflow.

The anomalously warm Nordic Seas surface state associated with strong Iceland-Scotland overflow seems to a large extent to be caused by an increase in the oceanic heat transport across the ISR, which represents the main inflow region of warm subtropical water into the Nordic Seas. The correlation coefficient between the Iceland-Scotland overflow strength (positive out of Nordic Seas) and the heat transport across the ISR (positive into Nordic Seas) for the same lag-times as in Figs. 7 to 9 is about 0.8 in MPI-ESM, 0.7 in IPSLCM4 and 0.6 in BCM. The correlation between the Iceland-Scotland overflow strength and the North Atlantic ocean circulation indicates a strengthening of the gyre circulation in MPI-ESM (Fig. 7g for the subpolar gyre – SPG; note that for the cyclonic SPG negative values correspond to a strengthening of the gyre) and of the MOC at subpolar latitudes in BCM (Fig. 5c). A stronger North Atlantic ocean circulation transports more warm subtropical water northward. An anomalously warm surface state associated with strong Iceland-Scotland overflow is found downstream of the ISR along the path of the North Atlantic Current (NAC) in all three models (Figs. 7a, 8a and 9a). We note that the NAC path is different in the three models (Langehaug et al., 2012b).

To investigate whether the North Atlantic ocean circulation indeed influences the heat transport across the ISR, we have calculated the correlation between the heat transport and the barotropic streamfunction and MOC respectively (not shown). In MPI-ESM, the (zero-lag) correlation between the heat transport and the barotropic streamfunction closely resembles the one between the Iceland-Scotland overflow strength and the barotropic streamfunction (Fig. 7g), indicating a strengthening of the North Atlantic

CPD
10, 3255–3302, 2014

gyre circulation as well as a westward retreat of the SPG (with correlation coefficients up to 0.8) associated with strong heat transport. The retreat of the SPG could allow for a larger fraction of subtropical water to enter into the Nordic Seas (e.g. Hatun et al., 2005). We note that our results are nevertheless somewhat different from Hatun et al. (2005), who suggest that a westward retreat of the SPG is related to a weakening of the gyre circulation. Regarding the MOC, no significant positive correlation coefficients with the heat transport are found at zero-lag or with the MOC leading by a few years, suggesting that the increase in the heat transport across the ISR in MPI-ESM is mainly caused by the (strengthened and spatially modified) North Atlantic gyre circulation.

In BCM, the correlation between the heat transport across the ISR (lagging by a few years) and the barotropic streamfunction also exhibits a westward retreat of the SPG (with correlation coefficients up to 0.7) associated with strong heat transport. In addition, a weak (but significant) intergyre gyre pattern (Marshall et al., 2001) is found, indicating a northward shift of the gyre circulation associated with strong heat transport. Regarding the MOC, the correlation between heat transport and MOC resembles the one between Iceland-Scotland overflow strength and MOC (Fig. 5c), with significant, although weak, positive correlation coefficients, when the MOC at subpolar latitudes leads the heat transport by a few years. Thus, both gyre circulation and MOC can contribute to the increase in the heat transport across the ISR in BCM. In IPSLCM4, in contrast, no significant correlation coefficients indicating an influence of the gyre and overturning component of the oceanic circulation on the heat transport are found, leaving the reason for the increase in the heat transport across the ISR and the anomalously warm surface state along the NAC path associated with strong Iceland-Scotland overflow unclear.

Regarding the surface heat flux in the Nordic Seas, the correlation with the Iceland-Scotland overflow strength (not shown) for the same lag-times as in Figs. 7 to 9 indicates mainly a damping effect on the Nordic Seas SST, with the exception of the southeastern part of the Nordic Seas in IPSLCM4. Thus, local air-sea interactions do, in general, not contribute to the anomalously warm Nordic Seas surface state

CPD
10, 3255–3302, 2014

associated with strong Iceland-Scotland overflow. In contrast, the correlation between the Iceland-Scotland overflow strength and the surface fresh water flux (not shown) for the same lag-times as in Figs. 7 to 9 indicates a net surface fresh water loss, which contributes to the anomalously salty Nordic Seas surface state associated with strong Iceland-Scotland overflow in MPI-ESM and IPSLCM4. In BCM, a net surface fresh water loss, which contributes to the anomalously salty surface state, is only found in the eastern part of the Nordic Seas. The western part, where a net surface fresh water gain is counteracting the anomalously salty surface state, is discussed below. The net surface fresh water loss associated with strong Iceland-Scotland overflow in MPI-ESM, IPSLCM4 and the eastern part of the Nordic Seas in BCM is caused by increased evaporation in all three models (Figs. 7c, 8c and 9c). Increased precipitation over the Nordic Seas is found for strong Iceland-Scotland overflow in all three models (not shown), counteracting the effect of evaporation. Sea ice melting will also counteract the effect of evaporation, as warm conditions lead to a decrease in sea ice (not shown). We note that the Nordic Seas SSS anomalies created by evaporation anomalies could be related to the Nordic Seas SST anomalies, as a warm surface state tends to increase the moisture gradient between the sea surface and the overlying atmosphere. This effect has not been quantified here, but it is generally weak at high latitudes.

In BCM, in the western part of the Nordic Seas, the combined effect of sea ice melting and increased precipitation is larger than the effect of increased evaporation, leading to a net surface fresh water gain (not shown). The anomalously salty surface state in the western part of the Nordic Seas associated with strong Iceland-Scotland overflow (Fig. 9b) can be related to the strength of the MOC. The correlation between the maximum strength of the North Atlantic MOC and the North Atlantic SSS in BCM (not shown) closely resembles the correlation between the maximum strength of the North Atlantic MOC and the North Atlantic SST (Fig. 6f), while no significant correlation coefficients between the maximum strength of the North Atlantic MOC and the Nordic Seas SSS are found in the other two models (with the exception of the Norwegian coastal area in MPI-ESM). The dynamical explanation for the correlation between the

CPD
10, 3255–3302, 2014

MOC strength and the western Nordic Seas SSS in BCM is, however, not clear. The salt transport into the Nordic Seas (across the ISR), which provides the most plausible explanation for an influence of the MOC strength on the Nordic Seas SSS, significantly correlates with the SSS only in the eastern part of the Nordic Seas (not shown).

Regarding the salt transport across the ISR, correlation coefficients with the Iceland-Scotland overflow strength (not shown) for the same lag-times as in Figs. 7 to 9 are smaller than the correlation coefficients between the Iceland-Scotland overflow strength and the heat transport across the ISR. They are well above the significance level only in IPSLCM4. In contrast to SST, where positive correlation coefficients with the Iceland-Scotland overflow strength are found both north and south of the ISR, no significant positive correlation coefficients are found for SSS downstream of the ISR along the NAC path in all three models (Figs. 7b, 8b and 9b). These findings are consistent with the fact that the anomalously salty surface state in the eastern part of the Nordic Seas associated with strong Iceland-Scotland overflow is caused by local air-sea interactions rather than anomalous oceanic salt transport in all three models.

The Nordic Seas SST and SSS anomalies associated with the anomalies in the Iceland-Scotland overflow strength generally have a counteracting effect on the surface density (Figs. 7d, 8d and 9d), except for the northwestern part in MPI-ESM and IPSLCM4 and along the Norwegian coast in MPI-ESM. In MPI-ESM (Fig. 7d), the surface density anomalies in the eastern part of the Nordic Seas (which is important for the Iceland-Scotland overflow strength as discussed below) are dominated by the temperature anomalies, resulting in anomalously light surface water associated with strong Iceland-Scotland overflow. In contrast, in IPSLCM4 (Fig. 8d) and BCM (Fig. 9d) the surface density anomalies in the (central) Nordic Seas are dominated by the salinity anomalies, resulting in anomalously dense surface water associated with strong Iceland-Scotland overflow.

As a consequence of the decrease in surface density in the northeastern part of the Nordic Seas in MPI-ESM (Fig. 7d), the convective activity, defined by the mixed layer depth in March, is reduced associated with strong Iceland-Scotland overflow

CPD
10, 3255–3302, 2014

(Fig. 7e). This finding is consistent with Jungclaus et al. (2005), who show that in the MPI coupled model the upper-ocean density anomalies associated with Nordic Seas convection are dominated by temperature anomalies. As a consequence of reduced convection, a deepening of the deep isopycnals in the northeastern part of the Nordic Seas is found in MPI-ESM (Fig. 7f). The isopycnal, on which the correlation coefficients shown in Figs. 7f, 8f and 9f are based, represents the threshold isopycnal used to calculate the Iceland-Scotland overflow strength in the models, as described in Sect. 2.2. We note that a deepening of the deep isopycnals associated with strong Iceland-Scotland overflow can also be caused/enhanced by more removal of dense water from the Nordic Seas due to strong overflow itself (Olsen et al., 2008). The reduction in the doming structure of the Nordic Seas isopycnals in MPI-ESM goes along with an anticyclonic circulation anomaly (Fig. 7g) as well as anomalously high sea surface height (SSH, Fig. 7h) in the northeastern part of the Nordic Seas. Anomalously high SSH is also found along the Norwegian coast and the ISR, with similar correlation coefficients as found in the northeastern part of the Nordic Seas. The anomalously high SSH along the Norwegian coast and the ISR can (partly) be related to the expansion of the water column due to the anomalously light surface water found in this region (Fig. 7d).

In IPSLCM4 and BCM, on the other hand, the increase in surface density in the central Nordic Seas associated with strong Iceland-Scotland overflow leads to an increase in convective activity (Figs. 8e and 9e) and consequently to a shallowing of the deep isopycnals in the central Nordic Seas (Figs. 8f and 9f). The increase in the doming structure of the isopycnals goes along with a cyclonic circulation anomaly (Figs. 8g and 9g) as well as anomalously low SSH (Figs. 8h and 9h) in the central Nordic Seas. Along the Norwegian coast and the ISR, on the contrary, a deepening of the deep isopycnals and anomalously high SSH are associated with strong Iceland-Scotland overflow, especially in BCM. In IPSLCM4, these anomalies are rather weak. As discussed above, a deepening of the isopycnals is dynamically consistent with the anomalously high SSH, but can also be caused/enhanced by more removal of dense

CPD
10, 3255–3302, 2014

water from the Nordic Seas due to strong overflow itself. The anomalously high SSH in IPSLCM4 can be related to the anomalously light surface water along the Norwegian coast and the ISR (Fig. 8d), similar to MPI-ESM. Also in BCM, anomalously light surface water is found along the Norwegian coast and the ISR. However, correlation coefficients are mainly not significant (Fig. 9d).

In BCM, the anomalously high SSH along the Norwegian coast associated with strong Iceland-Scotland overflow is mainly caused by increased northward wind stress over the eastern part of the Nordic Seas (Fig. 9i). Maximum correlation coefficients between the Iceland-Scotland overflow strength and the meridional wind stress component reach up to 0.7, which is at the upper end of correlation coefficients found in BCM between the Iceland-Scotland overflow strength and oceanic and atmospheric quantities in the Nordic Seas region (Fig. 9). These wind stress anomalies contribute, via increased Ekman transport towards the Norwegian coast, to the anomalously high SSH. In the other two models, such wind stress anomalies are not seen (Figs. 7i and 8i).

According to the literature (e.g. Hansen and Østerhus, 2007; Jungclaus et al., 2008; Olsen et al., 2008; Sandø et al., 2012), the overflow transport through the FSC is affected by the pressure gradient across the ISR in the core depth of the overflow. In MPI-ESM and BCM, the overflow transport across the ISR is restricted to the FSC; in IPSLCM4, the FSC overflow carries the majority of the overflow transport across the ISR. Thus, we assume that the Iceland-Scotland overflow strength, on which Figs. 7 to 9 are based, is affected by the pressure gradient across the ISR. Possible explanations for strong Iceland-Scotland overflow associated with an anomalously warm and salty Nordic Seas surface state in the three models are as follows:

In MPI-ESM, anomalously high SSH in the Nordic Seas (Fig. 7h) leads to an increase in the (barotropic) pressure north of the ISR. Significant correlation coefficients between the Iceland-Scotland overflow strength and the SSH are also found south of the ridge. However, sensitivity experiments performed with a coarser-resolution version of MPI-ESM and no external forcing (Lohmann et al., 2014) suggest that the

CPD
10, 3255–3302, 2014

low-frequency variability of the Iceland-Scotland overflow strength can be suppressed when climatological hydrography (temperature and salinity) is prescribed in the Nordic Seas and along the ISR, but full hydrographic variability is used south of the ridge. This indicates that the SSH anomalies north (and at) the ridge are sufficient to determine the low-frequency variability of the Iceland-Scotland overflow strength. Furthermore, Olsen et al. (2008), analysing a simulation with the ocean component of MPI-ESM (with the same grid configuration as used in our study) forced with atmospheric reanalysis fields, link the variability of the Iceland-Scotland overflow strength mainly to anomalous SSH in the Nordic Seas. Thus, we speculate that a strong Iceland-Scotland overflow in MPI-ESM is (mainly) caused by the anomalously high SSH north of the ISR.

In IPSLCM4, an increase in the doming of the deep isopycnals in the Nordic Seas (Fig. 8f) leads to an increase in the (baroclinic) pressure north of the ISR, causing a strengthened Iceland-Scotland overflow. In BCM, both increased (baroclinic) pressure in the central Nordic Seas due to an increase in the doming of the deep isopycnals (Fig. 9f) as well as increased (barotropic) pressure along the Norwegian coast due to anomalously high SSH (Fig. 9h) can contribute to a strengthened Iceland-Scotland overflow. The relative importance of the two processes is, however, difficult to estimate based on statistical analysis alone. As discussed above, the SSH anomalies along the Norwegian coast are related to the wind stress rather than the Nordic Seas surface state. The possible influence of the wind stress on the Iceland-Scotland overflow strength in BCM might explain, why the correlation coefficients between the Iceland-Scotland overflow strength and the Nordic Seas surface state are weaker compared to the other two models (Figs. 7a, b, 8a, b and 9a, b).

From the results presented in this section we conclude that mechanism (ii), an influence of the Nordic Seas SST, which is positively correlated with the AMO index, on the Iceland-Scotland overflow strength, provides a possible explanation for the (simulated) in-phase variation of Iceland-Scotland overflow strength and AMO index.

CPD
10, 3255–3302, 2014

4 Discussion

In this study we use simulations of the last millennium driven by external forcing reconstructions with three coupled climate models to investigate the two mechanisms proposed in the introduction as possible explanation for the covarying of Iceland-Scotland overflow strength and AMO index. Similar variability of the two time series has been suggested from paleo-reconstructions (Mjell et al., 2014a) and is also largely found in the model simulations. Mechanism (i) is based on a large-scale link through the strength of the MOC, while mechanism (ii) is based on a more local link through the influence of the Nordic Seas SST on the Iceland-Scotland overflow strength. Mechanism (ii) also involves the large-scale North Atlantic ocean circulation through the northward transport of heat and salt along the NAC path, which affects the Nordic Seas surface state.

In the model simulations, we do not find evidence for a robust relation between the Iceland-Scotland overflow strength and the MOC in the sense that a strong [weak] overflow is leading a strong [weak] MOC. The simulated influence of the Iceland-Scotland overflow strength on the MOC might, however, be underestimated, as the models do not realistically simulate the flow path of the Iceland-Scotland overflow water south of the ISR. The (simulated) basinwide AMO index is dominated by the low-latitude SST variability, which is strongly influenced by the external forcing, in particular long lasting effects of major volcanic eruptions (e.g. Otterå et al., 2010; Mignot et al., 2011; Zanchettin et al., 2012). Similar to their conclusions, our analysis indicates that the (simulated) basinwide AMO index is not predominantly an expression of MOC variations. This result is different from studies based on control simulations where multidecadal North Atlantic SST anomalies, as reflected in the AMO index, are associated with multidecadal MOC variations (e.g. Delworth and Mann, 2000; Latif et al., 2004; Knight et al., 2005; Zanchettin et al., 2013b). We conclude that mechanism (i) is not sufficient to explain the (simulated) in-phase variation of Iceland-Scotland overflow strength and AMO index.

CPD
10, 3255–3302, 2014

Rather, Iceland-Scotland overflow strength and AMO index are (in the simulations) linked through mechanism (ii). The Nordic Seas SST, which is positively correlated with the basinwide AMO index, affects, via convective activity, the isopycnal structure, barotropic circulation and SSH in the Nordic Seas, and consequently the baroclinic and barotropic pressure north of the ISR. According to the literature (e.g. Hansen and Østerhus, 2007; Jungclaus et al., 2008; Olsen et al., 2008; Sandø et al., 2012), the pressure gradient across the ISR influences the strength of the Iceland-Scotland overflow. Since the AMO index has no direct influence on the Iceland-Scotland overflow strength, mechanism (ii) crucially depends on the covariation of AMO index and Nordic Seas SST (as for the simulations shown in the left panels in Fig. 6). The question arises whether such a relation also exists in the real world. This question cannot be answered based on (paleo)observations, as, except for the last decades, SST observations in the Nordic Seas are too sparse to reasonably estimate the low-frequency SST variability in the Nordic Seas.

As an attempt to answer this question, we use a simulation with the ocean component of MPI-ESM forced with atmospheric reanalysis fields extending back to year AD 1870 (Compo et al., 2011). The simulation is described in detail in Müller et al. (2014). Figure 10 shows the simulated AMO index, defined as described in Sect. 2.2, together with the reconstructed AMO index from Gray et al. (2004). The two time series agree rather well, indicating that the ocean-only simulation realistically captures the low-frequency variability in the North Atlantic. We note, however, that the two time series are not independent from each other, since SST observations for the last ~ 150 years are used as boundary condition for the atmospheric reanalysis as well as to calibrate the reconstructed AMO index. Regarding the relation between AMO index and Nordic Seas SST, the ocean-only simulation is too short to estimate significant correlation coefficients between these two quantities, especially when a 21-year running mean lowpass filter is applied. Instead, in Fig. 10 we also show the simulated SST averaged over the Nordic Seas region. The low-frequency variability

CPD
10, 3255–3302, 2014

of the Nordic Seas SST generally agrees with the AMO index, suggesting that a covariation of AMO index and Nordic Seas SST exists also in the real world.

The details of the discussed mechanisms vary between the different models, underlining, on one hand, the importance of multi-model studies, but, on the other hand, also raising the question of realism of climate model simulations and imposing some uncertainty on the mechanism underlying the in-phase variation of Iceland-Scotland overflow strength and AMO index in the real world.

One major difference is the dependence of the Nordic Seas surface density anomalies associated with the Iceland-Scotland overflow strength on either temperature (MPI-ESM, eastern part of Nordic Seas, Fig. 7) or salinity (IPSLCM4 and BCM, Figs. 8 and 9). The reason for this difference is not clear; possible explanations are differences in the background surface state or in the amplitude of the low-frequency SST and SSS variability in the Nordic Seas. Regarding MPI-ESM and IPSLCM4, the latter exhibits a colder and fresher mean surface state in the eastern part of the Nordic Seas (not shown). Differences amount to 2–3 °C for SST and about 0.5 psu for SSS. IPSLCM4 exhibits a cold mean state in the North Atlantic in general (Marti et al., 2010, based on control simulations). The two model simulations also differ with respect to the amplitude of the low-frequency surface state variability in the eastern part of the Nordic Seas, determined from the standard deviation of 21-year running mean lowpass filtered time series (not shown). For SST, the variability is larger in MPI-ESM, while for SSS, larger variability is found in IPSLCM4. MPI-ESM and BCM, on the other hand, exhibit a relatively similar Nordic Seas surface state, both with respect to mean and standard deviation (not shown). Previous studies have shown that also subpolar surface density anomalies (related to decadal MOC variability) in different models depend on either temperature (e.g. Bentsen et al., 2004; Zhu and Jungclaus, 2008; Lohmann et al., 2009) or salinity (e.g. Delworth et al., 1993; Dong and Sutton, 2005; Mignot and Frankignoul, 2005; Msadek and Frankignoul, 2009). The reason for this difference is not clear from the literature. Langehaug et al. (2012b), analysing control simulations with BCM, IPSLCM4 and a coarser-resolution MPI-ESM configuration, suggest that

CPD
10, 3255–3302, 2014

differences in sea ice cover and NAC path contribute to differences in water mass transformation in the subpolar North Atlantic (which depends on density) in the three models. Understanding the difference in (North Atlantic) density anomalies in different models is a topic of much interest, but is beyond the scope of our study.

The difference in the mechanism, which possibly explains the anomalous overflow strength, is related to the difference in whether the surface density anomalies are temperature or salinity driven. Based on the assumption that the pressure gradient across the ISR affects the Iceland-Scotland overflow strength, in MPI-ESM, anomalies in the Iceland-Scotland overflow strength are associated with anomalous SSH in the Nordic Seas affecting the barotropic pressure. The importance of the barotropic pressure is in accordance with Olsen et al. (2008), analysing an ocean-only simulation with the ocean component of MPI-ESM (with the same grid configuration as used in our study) forced with atmospheric reanalysis fields. In contrast, in IPSLCM4 and BCM, anomalies in the Iceland-Scotland overflow strength are associated with anomalous doming of the isopycnals in the Nordic Seas affecting the baroclinic pressure. The importance of the baroclinic pressure has been suggested by e.g. Jungclaus et al. (2008).

In BCM, anomalous Iceland-Scotland overflow strength is also associated with anomalously high SSH along the Norwegian coast affecting the barotropic pressure. Sandø et al. (2012), analysing an ocean-only simulation with a regional version of the ocean component of BCM forced with atmospheric reanalysis fields, suggest that variations of the overflow transport through the FSC are mainly of barotropic nature. We note, however, that the dynamics underlying variations in the Iceland-Scotland overflow strength cannot be definitely determined from the statistical analysis discussed in Sect. 3.2. A more detailed understanding of the mechanisms explaining the variability of the Iceland-Scotland overflow strength in the three models is beyond the scope of our study, but nevertheless remains an important topic for future research.

Regarding the simulated in-phase variation of Iceland-Scotland overflow strength and AMO index, the correlation between the two time series is weaker in BCM, compared to the other two models (Fig. 4). Since the Nordic Seas surface state influences the strength of the Iceland-Scotland overflow, one possible explanation for this difference is the weaker correlation between the basinwide AMO index and the SST in the Nordic Seas in BCM compared to the other two models (left panels in Fig. 6). In BCM, the strength of the MOC affects the Nordic Seas SST (and SSS) to a much larger extent than in the other two models (right panels in Fig. 6). Our results for BCM are in agreement with Otterå et al. (2010), analysing the same BCM simulation as used in our study. They suggest that the external forcing is important only for the low-latitude SST variability, while the subpolar and Nordic Seas SST variability is strongly influenced by the MOC. Otterå et al. (2010) also show a significant out-of-phase relation between the AMO index and the strength of the MOC in the externally forced BCM simulation. The influence of the MOC on the Nordic Seas SST is therefore one possible reason for the weaker correlation between the AMO index and the Nordic Seas SST, and thus for the weaker correlation between the AMO index and the Iceland-Scotland overflow strength, in BCM.

In MPI-ESM and IPSLCM4, on the other hand, there is evidence for an influence of the external forcing on the Nordic Seas SST. In response to major volcanic eruptions, Zanchettin et al. (2012), analysing simulations of the last millennium with a coarser-resolution MPI-ESM configuration, find the largest North Atlantic upper ocean temperature anomalies in the Nordic Seas, partly caused by a reduced meridional oceanic heat transport. Mignot et al. (2011), analysing the same IPSLCM4 simulation as used in our study, describe a northward propagation of the tropical SST anomalies following major volcanic eruptions. In MPI-ESM and especially in IPSLCM4, the MOC signature on the North Atlantic SST (and SSS) in the externally forced simulations (Fig. 6b and d) is much weaker compared to the respective control simulation (not shown), in contrast to BCM, where the MOC signature on the North Atlantic surface state is similar in the externally forced (Fig. 6f) and the respective control simulation (not shown). The relatively strong influence of the external forcing on the Nordic Seas SST and the low-latitude SST in MPI-ESM and IPSLCM4 helps phasing the AMO

CPD
10, 3255–3302, 2014

index (dominated by the low-latitude SST variability) and the Iceland-Scotland overflow strength (influenced by the Nordic Seas surface state) in these two models, especially during periods of strong external forcing.

Apart from the MOC influence on the Nordic Seas surface state, another possible explanation for the less clear in-phase variation of Iceland-Scotland overflow strength and AMO index in BCM is the influence of the wind stress over the eastern part of the Nordic Seas on the Iceland-Scotland overflow strength in this model. Such an influence is not seen in the other two models. The wind stress anomalies over the eastern part of the Nordic Seas are not necessarily in phase with the low-latitude North Atlantic SST variability, as reflected in the AMO index, but can influence the Iceland-Scotland overflow strength by causing anomalously high SSH along the Norwegian coast as discussed in Sect. 3.2.

5 Conclusions

To summarize, the following main conclusions can be drawn from our study:

– Similar low-frequency variations of Iceland-Scotland overflow strength and AMO index, as suggested from paleo-reconstructions (Mjell et al., 2014a), can largely be seen in coupled climate model simulations of the last millennium driven by external forcing reconstructions.

– The basinwide AMO index in the externally forced simulations is dominated by the low-latitude SST variability, which according to the literature is strongly influenced by the external forcing, and is not predominantly driven by variations in the strength of the MOC.

– The simulated in-phase variation of Iceland-Scotland overflow strength and AMO index is based on the influence of the Nordic Seas SST, which is positively correlated with the AMO index, on the pressure north of the ISR. According to literature, the pressure gradient across the ISR affects the Iceland-Scotland overflow strength.

- The details of this mechanism differ between the different models, underlining the importance of multi-model analysis.
- Our study demonstrates that paleo-climate simulations provide a useful tool to understand mechanisms and large-scale connections associated with localized and rather sparse paleo-observations. With respect to paleo-climate simulations, the simulations of the last millennium performed within the framework of the CMIP5 and PMIP3 projects provide an excellent database for future studies.

Acknowledgements. This work was supported by the European Community's 7th framework programme (FP7/2007-2013) under grant agreement No. GA212643 (THOR: Thermohaline circulation – at risk?, 2008–2012). K. Lohmann also received funding through the Cluster of Excellence "CLISAP", funded by the German Science Foundation (DFG). D. Matei was supported by the Federal Ministry for Education and Research (BMBF) NORTH ATLANTIC and RACE projects. The authors wish to thank Davide Zanchettin for a critical review of the manuscript prior to submission. Fruitful discussions with colleagues at the Max Planck Institute for Meteorology are greatly acknowledged. The MPI-ESM simulation was conducted at the German Climate Computing Center (DKRZ). This study is a contribution to the Centre for Climate Dynamics at the Bjerknes Centre.

The service charges for this open access publication
have been covered by the Max Planck Society.

CPD
10, 3255–3302, 2014

References

Ammann, C., Meehl, G., Washington, W., and Zender, C.: A monthly and latitudinally varying volcanic forcing dataset in simulations of 20th century climate, Geophys. Res. Lett., 30, 1657, doi:10.1029/2003GL016875, 2003.

Ba, J., Keenlyside, N., Latif, M., Park, W., Ding, H., Lohmann, K., Mignot, J., Menary, M., Otterå, O. H., Wouters, B., Salas, D., Oka, A., Belluci, A., and Volodin, E.: A multi-model comparison for Atlantic multidecadal variability, Clim. Dynam., doi:10.1007/s00382-014-2056-1, in press, 2014.

Bentsen, M., Drange, H., Furevik, T., and Zhou, T.: Simulated variability of the Atlantic meridional overturning circulation, Clim. Dynam., 22, 701–720, 2004.

Bleck, R. and Smith, L.: A wind-driven isopycnic coordinate model of the north and equatorial Atlantic Ocean, 1. Model development and supporting experiments, J. Geophys. Res., 95, 3273–3285, 1990.

Bleck, R., Rooth, C., Hu, D., and Smith, L.: Salinity-driven thermocline transients in a wind- and thermohaline-forced isopycnic coordinate model of the North Atlantic, J. Phys. Oceanogr., 22, 1486–1505, 1992.

Boessenkool, K., Hall, I., Elderfield, H., and Yashayaev, I.: North Atlantic climate and deep-ocean flow speed changes during the last 230 years, Geophys. Res. Lett., 34, L13614, doi:10.1029/2007GL030285, 2007.

Compo, G. P., Whitaker, J. S., Sardeshmukh, P. D., Matsui, N., Allan, R. J., Yin, X., Gleason, B. E., Vose, R. S., Rutledge, G., Bessemoulin, P., Brönnimann, S., Brunet, M., Crouthamel, R. I., Grant, A. N., Groisman, P. Y., Jones, P. D., Kruk, M. C., Kruger, A. C., Marshall, G. J., Maugeri, M., Mok, H. Y., Nordli, Ø., Ross, T. F., Trigo, R. M., Wang, X. L., Woodruff, S. D., and Worley, S. J.: The Twentieth Century Reanalysis Project, Q. J. Roy. Meteorol. Soc., 137, 1–28, doi:10.1002/qj.776, 2011.

Crowley, T. J., Baum, S. K., Kim, K.-Y., Hegerl, G. C., and Hyde, W. T.: Modeling ocean heat content changes during the last millennium, Geophys. Res. Lett., 30, 1932, doi:10.1029/2003GL017801, 2003.

Crowley, T. J., Zielinski, G., Vinther, B., Udisti, R., Kreutz, K., Cole-Dai, J., and Castellano, J.: Volcanism and the Little Ice Age, PAGES Newsletter, 16, 22–23, 2008.

Delworth, T. and Mann, M.: Observed and simulated multi-decadal variability in the Northern Hemisphere, Clim. Dynam., 16, 661–676, 2000.

Delworth, T., Manabe, S., and Stouffer, R.: Interdecadal variations of the thermohaline circulation in a coupled ocean-atmosphere model, J. Climate, 6, 1993–2011, 1993.
Déqué, M., Dreveton, C., Braun, A., and Cariolle, D.: The ARPEGE/IFS atmosphere model: A contribution to the French community climate modelling, Clim. Dynam., 10, 249–266, 1994.
Dong, B. and Sutton, R.: Mechanism of interdecadal thermohaline circulation variability in a coupled ocean-atmosphere GCM, J. Climate, 18, 1117–1135, 2005.
Dukowicz, J. and Baumgardner, J.: Incremental remapping as a transport/advection algorithm, J. Comput. Phys., 160, 318–335, 2000.
Fichefet, T. and Maqueda, M. A. M.: Sensitivity of a global sea ice model to the treatment of ice thermodynamics and dynamics, J. Geophys. Res., 102, 12609–12646, 19970
Furevik, T., Bentsen, M., Drange, H., Kindem, I., Kvamstø, N., and Sorteberg, A.: Description and evaluation of the Bergen climate model: ARPEGE coupled with MICOM, Clim. Dynam., 21, 27–51, 2003.
Gao, C., Robock, A., and Ammann, C.: Volcanic forcing of climate over the last 1500 years: An improved ice-core based index for climate models, J. Geophys. Res., 113, D2311, doi:10.1029/2008JD010239, 2008
Gastineau, G. and Frankignoul, C.: Cold-season atmospheric response to the natural variability of the Atlantic meridional overturning circulation, Clim. Dynym., 39, 37–57, 2012.
Goosse, H. and Renssen, H.: Regional response of the climate system to solar forcing: the role of the ocean, Space Sci. Rev., 125, 227–235, 2006.
Gray, S., Graumlich, L., Betancourt, J., and Pederson, G.: A tree-ring based reconstruction of the Atlantic multidecadal oscillation since 1567 A.D., Geophys. Res. Lett., 31, L12205, doi:10.1029/2004GL019932, 2004.
Hansen, B. and Østerhus, S.: Faroe Bank Channel overflow 1995–2005, Prog. Oceanogr., 75, 817–856, 2007.
Hansen, B., Turrell, W., and Østerhus, S.: Decreasing overflow from the Nordic seas into the Atlantic Ocean through the Faroe Bank channel since 1950, Nature, 411, 927–930, 2001.
Hansen, B., Østerhus, S., Turrell, B., Jónsson, S., Valdimarsson, H., Hátún, H., and Olsen, S.: The inflow of Atlantic water, heat, and salt to the Nordic Seas across the Greenland-Scotland Ridge, in: Arctic–Subarctic Ocean Fluxes: Defining the role of the Northern Seas in Climate, edited by: Dickson, D., Meincke, J., and Rhines, P., Springer Verlag, Dordrecht, 2008.
Hatun, H., Sandø, A. B., Drange, H., Hansen, B., and Valdimarsson, H.: Influence of the Atlantic subpolar gyre on the thermohaline circulation, Science, 309, 1841–1844, 2005.

CPD
10, 3255–3302, 2014

Hourdin, F., Musat, I., Bony, S., Braconnot, P., Codron, F., Dufresne, J., Fairhead, L., Filiberti, M. A., Friedlingstein, P., Grandpeix, J. Y., Krinner, G., Levan, P., Li, Z., and Lott, F.: The LMDZ4 general circulation model: climate performance and sensitivity to parametrized physics with emphasis on tropical convection, Clim. Dynym., 27, 787–813, 2006.

Ilyina, T., Six, K. D., Segschneider, J., Maier-Reimer, E., Li, H., and Núñez-Riboni, I.: Global ocean biogeochemistry model HAMOCC: Model architecture and performance as component of the MPI-Earth System Model in different CMIP5 experimental realizations, J. Adv. Model. Earth Syst., 5, 287–315, 2013.

Jungclaus, J. H., Haak, H., Latif, M., and Mikolajewicz, U.: Arctic–North Atlantic interactions and multidecadal variability of the meridional overturning circulation, J. Climate, 18, 4013–4031, 2005.

Jungclaus, J. H., Macrander, A., and Käse, R.: Modelling the overflows across the Greenland-Scotland Ridge, in: Arctic–Subarctic Ocean Fluxes: Defining the role of the Northern Seas in Climate, edited by: Dickson, R., Meincke, J., and Rhines, P., Springer Verlag, Dordrecht, 2008.

Jungclaus, J. H., Lorenz, S. J., Timmreck, C., Reick, C. H., Brovkin, V., Six, K., Segschneider, J., Giorgetta, M. A., Crowley, T. J., Pongratz, J., Krivova, N. A., Vieira, L. E., Solanki, S. K., Klocke, D., Botzet, M., Esch, M., Gayler, V., Haak, H., Raddatz, T. J., Roeckner, E., Schnur, R., Widmann, H., Claussen, M., Stevens, B., and Marotzke, J.: Climate and carbon-cycle variability over the last millennium, Clim. Past, 6, 723–737, doi:10.5194/cp-6-723-2010, 2010.

Jungclaus, J. H., Fischer, N., Haak, H., Lohmann, K., Marotzke, J., Matei, D., Mikolajewicz, U., Notz, D., and von Storch, J. S.: Characteristics of the ocean simulations in Max Planck Institute Ocean Model (MPIOM), the ocean component of the MPI-Earth System Model, J. Adv. Model. Earth Syst., 5, 422–446, 2013.

Knight, J., Allan, R., Folland, C., Vellinga, M., and Mann, M.: A signature of persistent natural thermohaline circulation cycles in observed climate, Geophys. Res. Lett., 32, L20708, doi:10.1029/2005GL024233, 2005.

Köhl, A. and Stammer, D.: Variability of the meridional overturning in the North Atlantic from the 50-year GECCO state estimate, J. Phys. Oceanogr., 38, 1913–1930, 2008.

Krinner, G., Viovy, N., de Noblet-Ducoudre, N., Ogee, J., Polcher, J., Friedlingstein, P., Ciais, P., Sitch, S., and Prentice, I. C.: A dynamic global vegetation for studies

of the coupled atmosphere-biosphere system, Global Biogeochem. Cy., 19, GB1015, doi:10.1029/2003GB002199, 2005.
Langehaug, H. R., Medhaug, I., Eldevik, T., and Ottera, O. H.: Arctic/Atlantic exchanges via the subpolar gyre, J. Climate, 25, 2421–2439, 2012a.
Langehaug, H. R., Rhines, P. B., Eldevik, T., Mignot, J., and Lohmann, K.: Water mass transformation and the North Atlantic Current in three multicentury climate model simulations, J. Geophys. Res., 117, C11001, doi:10.1029/2012JC008021, 2012b.
Latif, M., Roeckner, E., Botzet, K., Esch, M., Haak, H., Hagemann, S., Jungclaus, J., Legutke, S., Marsland, S., Mikolajewicz, U., and Mitchell, J.: Reconstructing, monitoring and predicting decadal-scale changes in the North Atlantic thermohaline circulation with sea surface temperature, J. Climate, 17, 1605–1614, 2004.
Lohmann, K., Drange, H., and Bentsen, M.: Response of the North Atlantic subpolar gyre to persistent North Atlantic oscillation like forcing, Clim. Dynam., 32, 273–285, 2009.
Lohmann, K., Jungclaus, J. H., Matei, D., Mignot, J., Menary, M., Langehaug, H. R., Ba, J., Gao, Y. Q., Otterå, O. H., Park, W., and Lorenz, S.): The role of subpolar deep water formation and Nordic Seas overflows in simulated multidecadal variability of the Atlantic meridional overturning circulation, Ocean Sci., 10, 227–241, doi:10.5194/os-10-227-2014, 2014.
Madec, G., Delecluse, P., Imbard, M., and Levy, M.: OPA 8.1, ocean general circulation model reference manual. Notes du pole de modelisation, 11, Institut Pierre-Simon Laplace (IPSL), Paris, France, 91 pp., 1998.
Mann, M. E., Zhang, Z., Rutherford, S., Bradley, R. S., Hughes, M. K., Shindell, D., Ammann, C., Faluvegi, G., and Ni, F.: Global signatures and dynamical origins of the Little Ice Age and Medieval Climate Anomaly, Science, 326, 1256–1260, 2009.
Marshall, J., Johnson, H., and Godman, J.: A study of the interaction of the North Atlantic oscillation with ocean circulation, J. Climate, 14, 1399–1421, 2001.
Marsland, S., Haak, H., Jungclaus, J. H., Latif, M., and Röske, F.: The Max Planck Institute global ocean/sea ice model with orthogonal curvilinear coordinates, Ocean Modell., 5, 91–127, 2003.
Marti, O., Braconnot, P., Dufresne, J.-L., Bellier, J., Benshila, R., Bony, S., Brockmann, P., Cadule, P., Caubel, A., Codron, F., de Noblet, N., Denvil, S., Fairhead, L., Fichefet, T., Foujols, M.-A., Friedlingstein, P., Goosse, H., Grandpeix, J.-Y., Guilyardi, E., Hourdin, F., Idelkadi, A., Kageyama, M., Krinner, G., Lévy, C., Madec, G., Mignot, J., Musat, I., Swingedouw, D.,

and Talandier, C.: Key features of the IPSL ocean atmosphere model and its sensitivity to atmospheric resolution, Clim. Dynam., 34, 1–26, 2010.
Menary, M., Park, W., Lohmann, K., Vellinga, M., Palmer, M., Latif, M., and Jungclaus, J.: A multimodel comparison of centennial Atlantic meridional overturning circulation variability, Clim. Dynam., 38, 2377–2388, 2012.
Mignot, J. and Frankignoul, C.: On the variability of the Atlantic meridional overturning circulation, the North Atlantic Oscillation and the El Nino-Southern Oscillation in the Bergen Climate Model, J. Climate, 18, 2361–2375, 2005.
Mignot, J., Khodri, M., Frankignoul, C., and Servonnat, J.: Volcanic impact on the Atlantic Ocean over the last millennium, Clim. Past, 7, 1439–1455, doi:10.5194/cp-7-1439-2011, 2011.
Mjell, T. L., Ninnemann, U. S., Kleiven, H. F., and Hall, I. R.: Multidecadal changes in Iceland Scotland Overflow Water vigor over the last 600 years and its relationship to climate, Geophys. Res. Lett., submitted, 2014a.
Mjell, T. L., Langehaug, H. R., Otterå, O. H., Eldevik, T., Ninnemann, U. S., and Kleiven, H. F.: On the reconstruction of ocean circulation and climate based on the “Gardar Drift”, in preparation, 2014b.
Msadek, R. and Frankignoul, C.: Atlantic multidecadal oceanic variability and its influence on the atmosphere in a climate model, Clim. Dynam., 33, 45–62, 2009.
Müller, W. A., Matei, D., Bersch, M., Jungclaus, J. H., Haak, H., Lohmann, K., Compo, G., Sardeshmukh, P. D., and Marotzke, J.: A 20th-century reanalysis forced ocean model to reconstruct North Atlantic multi-decadal climate variability from 1872–2010, Clim. Dynam., submitted, 2014.
Myneni, R. B., Nemani, R. R., and Running, S. W.: Estimation of global leaf area index and absorbed par using radiative transfer models, IEEE T. Geosci. Remote., 35, 1380–1393, 1997.
Notz, D., Haumann, A., Haak, H., Jungclaus, J. H., and Marotzke, J.: Sea-ice evolution in the Arctic as modeled by Max Planck Institute for Meteorology’s Earth System Model, J. Adv. Model. Earth Syst., 5, 173–194, 2013.
Olsen, S. M., Hansen, B., Quadfasel, D., and Østerhus, S.: Observed and modeled stability of overflow across the Greenland–Scotland ridge, Nature, 455, 519–523, 2008.
Ortega, P., Montoya, M., González-Rouco, F., Mignot, J., and Legutke, S.: Variability of the Atlantic meridional overturning circulation in the last millennium and two IPCC scenarios, Clim. Dynam., 38, 1925–1947, 2012.

CPD
10, 3255–3302, 2014

Otterå, O. H., Bentsen, M., Bethke, I., and Kvamstø, N. G.: Simulated pre-industrial climate in Bergen Climate Model (version 2): model description and large-scale circulation features, Geosci. Model Dev., 2, 197–212, doi:10.5194/gmd-2-197-2009, 2009.

Otterå, O. H., Bentsen, M., Drange, H., and Suo, L.: External forcing as a metronome for Atlantic multidecadal variability, Nat. Geosci., 3, 688–694, 2010.

Park, W. and Latif, M.: Atlantic meridional overturning circulation response to idealized external forcing, Clim. Dynam., 39, 1709–1726, 2012.

Pongratz, J., Reick, C. H., Raddatz, T., and Claussen, M.: A Reconstruction of global agricultural areas and land cover for the last millennium, Global Biogeochem. Cy., 22, GB3018, doi:10.1029/2007GB003153, 2008.

Reick, C. H., Raddatz, T., Brovkin, V., and Gayler, V.: Representation of natural and anthropogenic land cover change in MPI-ESM, J. Adv. Model. Earth Syst., 5, 459–482, 2013.

Salas-Melia, D.: A global coupled sea ice-ocean model, Ocean Modell., 4, 137–172, 2002.

Sandø, A. B., Nilsen, J. E. Ø., Eldevik, T., and Bentsen, M.: Mechanisms for variable North Atlantic – Nordic Seas exchanges, J. Geophys. Res., 117, C12006, doi:10.1029/2012JC008177, 2012.

Schlesinger, M. E. and Ramankutty, N.: An oscillation in the global climate system of period 65–70 years, Nature, 367, 723–726, 1994.

Schmidt, G. A., Jungclaus, J. H., Ammann, C. M., Bard, E., Braconnot, P., Crowley, T. J., Delaygue, G., Joos, F., Krivova, N. A., Muscheler, R., Otto-Bliesner, B. L., Pongratz, J., Shindell, D. T., Solanki, S. K., Steinhilber, F., and Vieira, L. E. A.: Climate forcing reconstructions for use in PMIP simulations of the last millennium (v1.0), Geosci. Model Dev., 4, 33–45, doi:10.5194/gmd-4-33-2011, 2011.

Servonnat, J., Yiou, P., Khodri, M., Swingedouw, D., and Denvil, S.: Influence of solar variability, CO_2 and orbital forcing between 1000 and 1850 AD in the IPSLCM4 model, Clim. Past, 6, 445–460, doi:10.5194/cp-6-445-2010, 2010.

Stenchikov, G., Delworth, T. L., Ramswamy, V., Stouffer, R. J., Wittenberg, A., and Zeng, F.: Volcanic signals in oceans, J. Geophys. Res., 114, D16104, doi:10.1029/2008JD011673, 2009.

Stevens, B., Giorgetta, M., Esch, M., Mauritsen, T., Crueger, T., Rast, S., Salzmann, M., Schmidt, H., Bader, J., Block, K., Brokopf, R., Fast, I., Kinne, S., Kornblueh, L., Lohmann, U., Pincus, R., Reichler, T., and Roeckner, E.: Atmospheric component of the MPI-M Earth System Model (2013): ECHAM6, J. Adv. Model. Earth Syst., 5, 146–172, 2013.

CPD
10, 3255–3302, 2014

Using simulations of the last millennium to understand climate variability

K. Lohmann et al.

Swingedouw, D., Terray, L., Cassou, C., Voldoire, A., Salas-Melia, D., and Servonnat, J.: Natural forcing of climate during the last millennium: Fingerprint of solar variability and NAO, Clim. Dynam., 36, 1349–1364, 2011.

Terray, L.: Evidence for multiple drivers of North Atlantic multi-decadal climate variability, Geophys. Res. Lett., 39, L19712, doi:10.1029/2012GL053046, 2012.

Terray, L. and Thual, O.: Oasis: le couplage océan-atmosphére, La Météorologie, 10, 50–61, 1995.

Trenberth, K. and Shea, D.: Atlantic hurricanes and natural variability in 2005, Geophys. Res. Lett., 33, L12704, doi:10.1029/2006GL026894, 2006.

Valcke, S., Terray, L., and Piacentini, A.: Oasis 2.4, Ocean atmosphere sea ice soil: user's guide, Tech. Rep. TR/CMGC/00/10, CERFACS, Toulouse, France, 2000.

Valcke, S., Claubel, A., Declat, D., and Terray, L.: OASIS Ocean Atmosphere Sea Ice Soil user's guide, Tech. Rep. TR/CMGC/03/69, CERFACS, Toulouse, France, 2003.

Vieira, L. and Solanki, S.: Evolution of the solar magnetic flux on time scales of years to millennia, Astron. Astrophys., 509, A100, doi:10.1051/0004-6361/200913276, 2010.

Vieira, L., Solanki, S., Krivova, N., and Usoskin, I.: Evolution of the solar irradiance during the Holocene, Astron. Astrophys., 531, A6, doi:10.1051/0004-6361/201015843, 2011.

Wold, C.: Cenozoic sediment accumulation on drifts in the northern North Atlantic, Paleoceanography, 9, 917–941, 1994.

Zanchettin, D., Timmreck, C., Graf, H.-F., Rubino, A., Lorenz, S., Lohmann, K., Krüger, K., and Jungclaus, J. H.: Bi-decadal variability excited in the coupled ocean–atmosphere system by strong tropical volcanic eruptions, Clim. Dynam., 39, 419–444, 2012.

Zanchettin, D., Rubino, A., Matei, D., Bothe, O., and Jungclaus, J. H.: Multidecadal-to-centennial SST variability in the MPI-ESM simulation ensemble for the last millennium, Clim. Dynam., 40, 1301–1318, 2013a.

Zanchettin, D., Bothe, O., Müller, W. A., Bader, J., and Jungclaus, J. H.: Different flavors of the Atlantic Multidecadal Variability, Clim. Dynam., doi:10.1007/s00382-013-1669-0, in press, 2013b.

Zhong, Y., Miller, G. H., Otto-Bliesner, B. L., Holland, M. M., Bailey, D. A., Schneider, D. P., and Geirsdottir, A.: Centennialscale climate change from decadally-paced explosive volcanism: a couled sea ice-ocean mechanism, Clim. Dynam., 37, 2373–2387, 2011.

CPD
10, 3255–3302, 2014

Using simulations of the last millennium to understand climate variability

K. Lohmann et al.

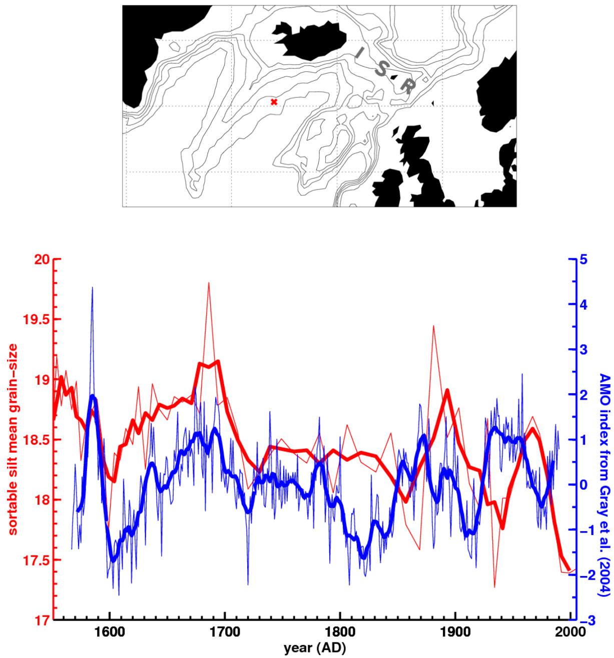

Figure 1. Reconstructed AMO index (normalized; blue lines) from Gray et al. (2004) and Iceland-Scotland overflow strength (in µm; red lines) from Mjell et al. (2014). The AMO index is shown as annual values (thin line) and with an 11-year running mean filter applied (thick line). For the Iceland-Scotland overflow strength, the original time series (thin line) has irregular dates and is smoothed by applying a 3-point running mean filter (thick line). The map shows the location of the sediment core on which the reconstructed Iceland-Scotland overflow strength is based (topography is shown for depths of 500, 1000, 1500, 2000 and 2500 m). Figure adapted from Mjell et al. (2014, their Fig. 2c).

CPD
10, 3255–3302, 2014

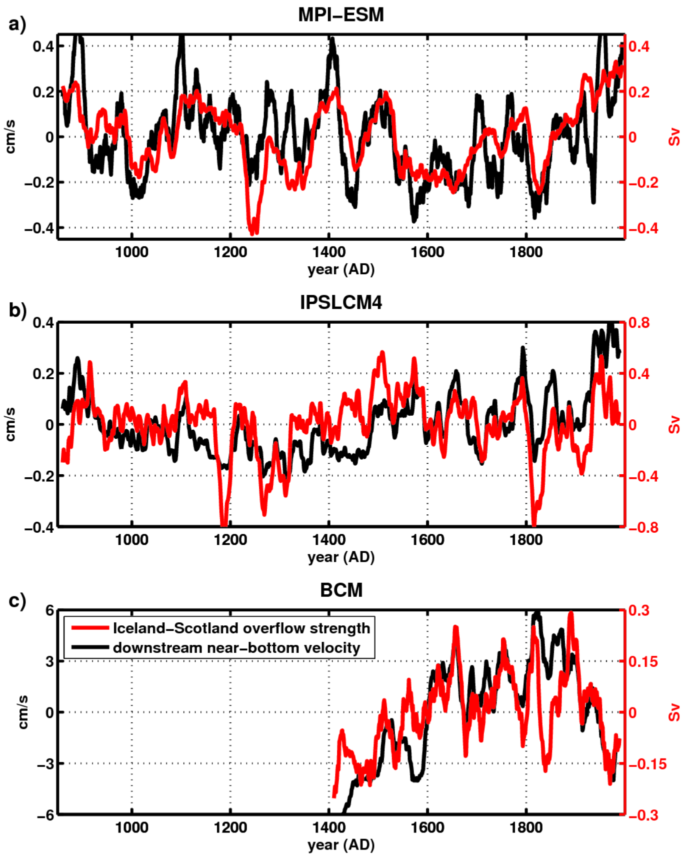

Figure 2. Simulated anomalous overflow transport across the ISR (red line; in Sv, 1 Sverdrup = 10^6 m^3 s^{-1}) and near-bottom flow speed $(u^2 + v^2)^{1/2}$ downstream of the ISR (black line; in cm s^{-1}) in MPI-ESM **(a)**, IPSLCM4 **(b)** and BCM **(c)**. All time series are annual values with a 21-year running mean filter applied.

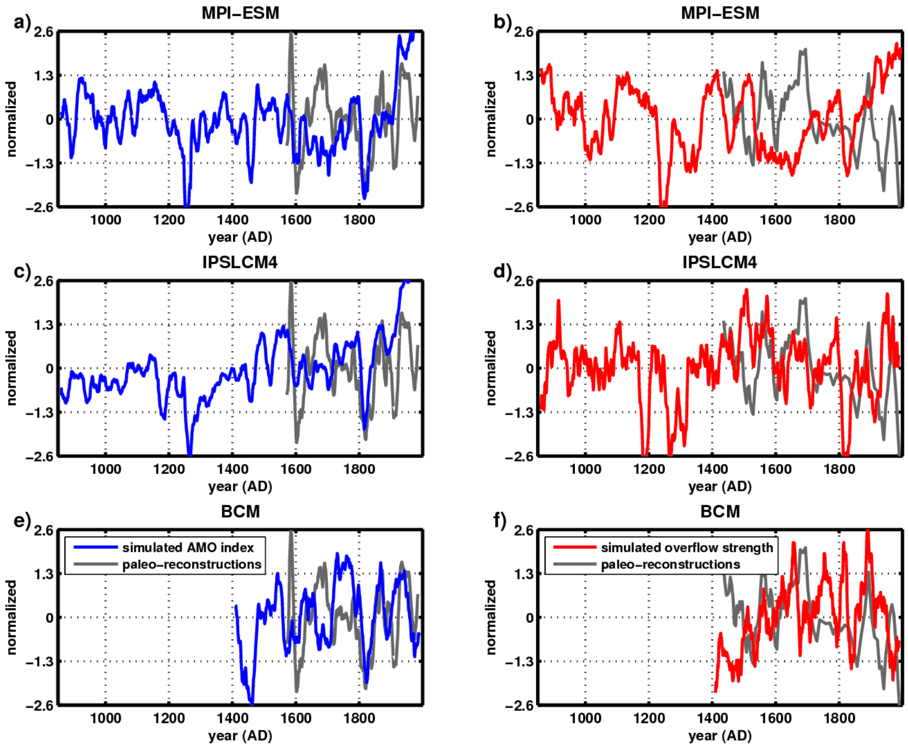

Figure 3. Left panels: anomalous simulated AMO index (blue line) in MPI-ESM **(a)**, IPSLCM4 **(c)** and BCM **(e)**, compared to the AMO reconstruction (grey line; same as thick blue line in Fig. 1) from Gray et al. (2004). Right panels: anomalous simulated overflow transport across the ISR (red line) in MPI-ESM **(b)**, IPSLCM4 **(d)** and BCM **(f)**, compared to the reconstructed Iceland-Scotland overflow strength (grey line; same as thick red line in Fig. 1) from Mjell et al. (2014). All time series are normalized by the respective standard deviation. Simulated time series are annual values with a 21-year running mean filter applied.

CPD
10, 3255–3302, 2014

Using simulations of the last millennium to understand climate variability

K. Lohmann et al.

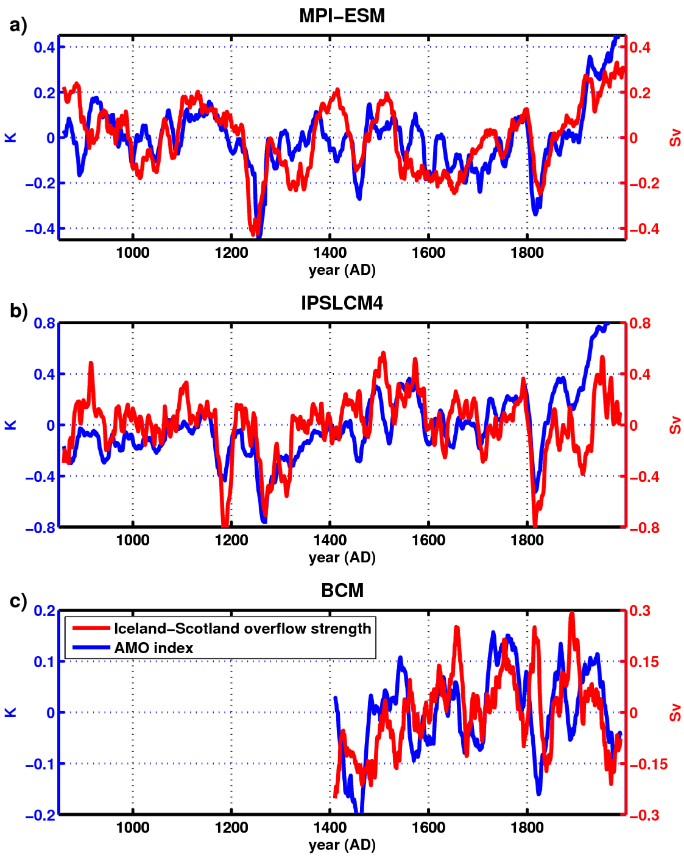

Figure 4. Simulated anomalous AMO index (blue line; in K) and overflow transport across the ISR (red line; in Sv) in MPI-ESM **(a)**, IPSLCM4 **(b)** and BCM **(c)**. All time series are annual values with a 21-year running mean filter applied.

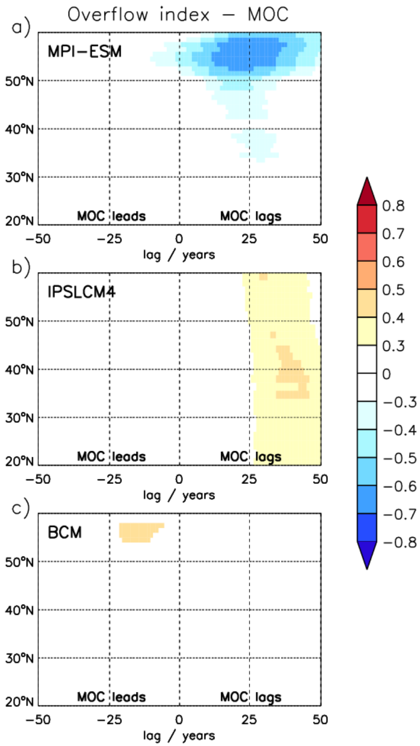

Figure 5. Lag correlation coefficients between the Iceland-Scotland overflow strength and the strength of the MOC at the different latitudes in the North Atlantic in MPI-ESM **(a)**, IPSLCM4 **(b)** and BCM **(c)**. The strength of the MOC is taken at the depth where the absolute maximum strength of the North Atlantic MOC is located (1000 m in MPI-ESM and BCM, 1200 m in IPSLCM4). The correlation analysis is based on annual values for the period AD 850 to 1849 (MPI-ESM, IPSLCM4) and AD 1550 to 1999 (BCM) with a 21-year running mean filter applied. Only correlation coefficients statistically significant at the 95 % confidence level are shown (significance level: 0.27 in MPI-ESM and IPSLCM4, 0.4 in BCM).

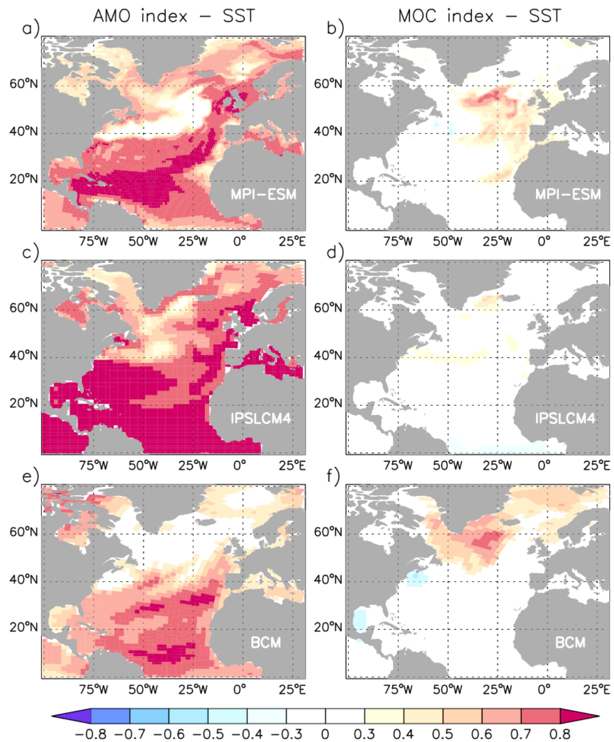

Figure 6. Left panels: correlation coefficients between the AMO index and the North Atlantic SST in MPI-ESM **(a)**, IPSLCM4 **(c)** and BCM **(e)**. Right panels: correlation coefficients between the maximum strength of the North Atlantic MOC and the North Atlantic SST in MPI-ESM **(b)**, IPSLCM4 **(d)** and BCM **(f)**. The MOC index is leading by four years in MPI-ESM and 12 years in BCM, otherwise zero lag is shown. The correlation analysis is based on annual values for the period AD 850 to 1849 (MPI-ESM, IPSLCM4) and AD 1550 to 1999 (BCM) with a 21-year running mean filter applied. Only correlation coefficients statistically significant at the 95 % confidence level are shown (significance level: 0.27 in MPI-ESM and IPSLCM4, 0.4 in BCM).

CPD
10, 3255–3302, 2014

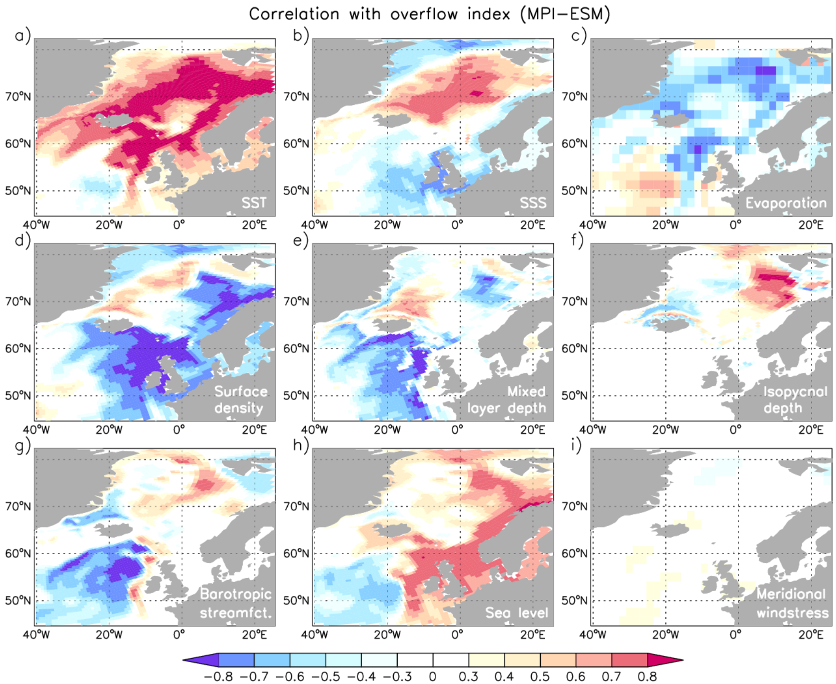

Figure 7. Correlation coefficients between the Iceland-Scotland overflow strength and **(a)** the SST, **(b)** the SSS, **(c)** the evaporation (positive downward), **(d)** the surface density, **(e)** the mixed layer depth in March, **(f)** the depth of the isopycnal $\sigma = 27.8\,\mathrm{kg\,m^{-3}}$, **(g)** the barotropic streamfunction, **(h)** the sea surface height (linearly detrended prior to the analysis to account for the non-closed water budget between the atmosphere and the ocean) and **(i)** the meridional wind stress component in MPI-ESM. All correlation coefficients are shown at zero lag. The correlation analysis is based on annual values for the period AD 850 to 1849 with a 21-year running mean filter applied. Only correlation coefficients statistically significant at the 95 % confidence level are shown (significance level: 0.27).

CPD
10, 3255–3302, 2014

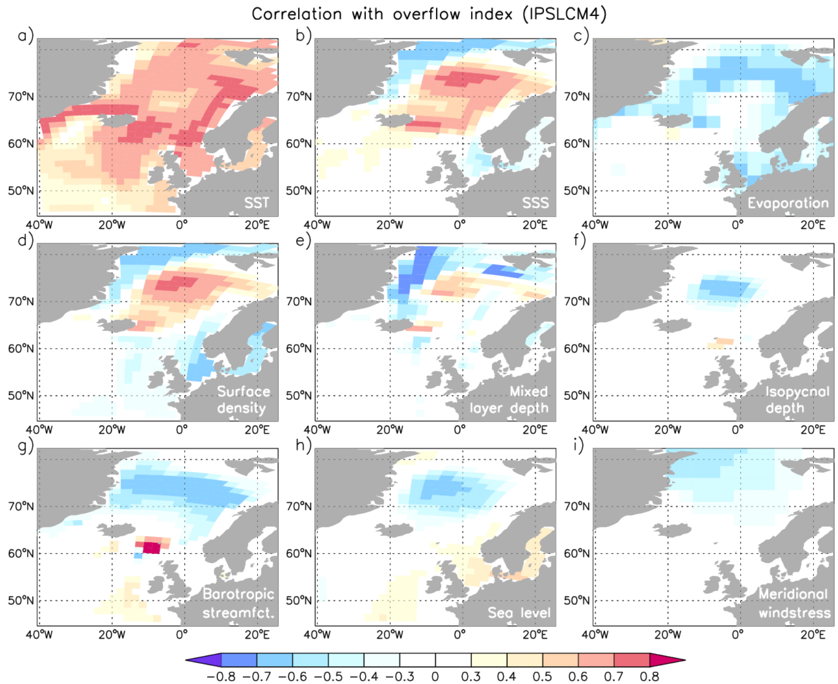

Figure 8. Correlation coefficients between the Iceland-Scotland overflow strength and **(a)** the SST, **(b)** the SSS, **(c)** the evaporation (positive downward), **(d)** the surface density, **(e)** the mixed layer depth in March, **(f)** the depth of the isopycnal $\sigma = 27.8\,\mathrm{kg\,m^{-3}}$, **(g)** the barotropic streamfunction, **(h)** the sea surface height and **(i)** the meridional wind stress component in IPSLCM4. All correlation coefficients are shown with the overflow strength lagging by two years. The correlation analysis is based on annual values for the period AD 850 to 1849 with a 21-year running mean filter applied. The data have been linearly detrended prior to the analysis to account for the model drift. Only correlation coefficients statistically significant at the 95 % confidence level are shown (significance level: 0.27).

CPD
10, 3255–3302, 2014

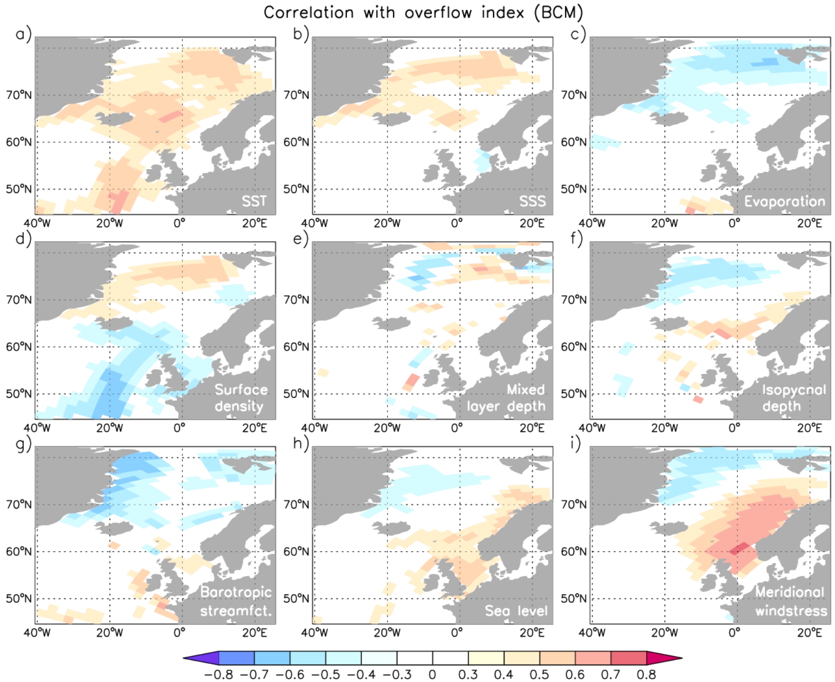

Figure 9. Correlation coefficients between the Iceland-Scotland overflow strength and **(a)** the SST, **(b)** the SSS, **(c)** the evaporation (positive downward), **(d)** the surface density, **(e)** the mixed layer depth in March, **(f)** the depth of the isopycnal $\sigma_2 = 36.946\,\mathrm{kg\,m^{-3}}$, **(g)** the barotropic streamfunction, **(h)** the sea surface height (linearly detrended prior to the analysis) and **(i)** the meridional wind stress component in BCM. All correlation coefficients are shown with the overflow strength lagging by nine years. The correlation analysis is based on annual values for the period AD 1550 to 1999 with a 21-year running mean filter applied. Only correlation coefficients statistically significant at the 95 % confidence level are shown (significance level: 0.4).

CPD
10, 3255–3302, 2014

Using simulations of the last millennium to understand climate variability

K. Lohmann et al.

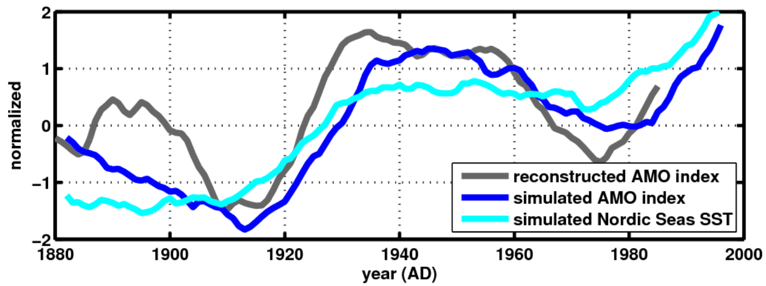

Figure 10. Reconstructed AMO index (grey line, same as thick blue line in Fig. 1) from Gray et al. (2004) as well as anomalous simulated AMO index (blue line) and Nordic Seas SST (averaged over the region 25° W–20° E, 60–80° N; cyan line) taken from an ocean-only simulation forced by atmospheric reanalysis fields. Simulated time series are annual values with a 21-year running mean filter applied. All time series are normalized by the respective standard deviation.

CPD
10, 3255–3302, 2014